J Korean Med Sci 1998; 13: 603-11
ISSN 1011-8934

Ultrastructural Changes of the Internal Elastic Lamina in Experimental Hypercholesterolemic Porcine Coronary Arteries

The internal elastic lamina (IEL) serves as a barrier for cells and macromolecules between the intima and media in the vascular wall. We evaluated the morphological changes and quantitative assessments of the IEL architecture in the coronary circulation of pigs fed with a high cholesterol diet. Transmission electron microscopy (TEM) analysis of the IEL from hypercholesterolemic coronary arteries revealed fragmentation of the IEL associated with a decrease in the thickness. Confocal microscopy and scanning electron microscopy (SEM) revealed an altered pattern characterized by a large oval fenestration in the IEL of hypercholesterolemic vessels. Morphometric analysis of confocal microscopy images demonstrated that the IEL of cholesterol-fed animals were characterized by an increase in the minor diameter of the fenestrae (2.16 ± 0.04 μm vs 3.32 ± 0.06 μm, p=0.003) and a decrease in the fenestrae density ($22,333 \pm 1,334/mm^2$ vs $17,552 \pm 931/mm^2$, p=0.015) compared to controls. The percentage of the IEL area covered by the fenestrae correlated with the intimal thickness (r=0.79, p=0.004). The immunoreactivity for matrix metalloproteinase-3 (MMP-3) increased in cholesterol-fed coronary arteries, predominantly in the neointima. This study demonstrates experimental hypercholesterolemia induced ultrastructural changes of the IEL in the coronary circulation. The IEL may play an important role in the development of structural changes which characterize the early phase of coronary atherosclerosis.

Key Words: *Elastic tissue, internal elastic lamina; Hypercholesterolemia, atherosclerosis; Microscopy, confocal; Stromelysin 1*

Hyuck Moon Kwon, Dongsoo Kim, Bum Kee Hong, Ki Hyun Byun, Soo Hwan Oh, Jun Sick Kna, Hyun-Seung Kim, Robert S. Schwartz,* Amir Lerman*

Department of Internal Medicine, College of Medicine, Yonsei University, Seoul, Korea
Departments of Internal Medicine and Cardiovascular Diseases, Mayo Clinic and Foundation, Rochester, MN, U.S.A.*

Received: June 2, 1998
Accepted: July 28, 1998

Address for correspondence
Hyuck Moon Kwon, M.D.
Department of Internal Medicine, Yonsei University, College of Medicine, 146-92, Dogok-dong, Kangnam-gu, Seoul 135-270, Korea
Tel: +82.2-3497-3330, Fax: +82.2-573-0112
E-mail: hmkwon@yumc.yonsei.ac.kr

INTRODUCTION

The arterial wall of all species, including humans, contains elastic laminae which were termed by Dees as the fenestrated membranes of Henle (1). The luminal surface of these laminae is a felt-like sheet composed of fine elastic fibers that merges into a coarse plexus of much larger elastic fibers. The IEL contains numerous small holes that vary in size and shape among arteries in the same species (2, 3). Two principal functions have been ascribed to the IEL, one supporting the vessel wall architecture and one providing a barrier between the intima and media layer (3).

Several studies have demonstrated discontinuities and abnormalities in the IEL structure of elastic arteries, such as the aorta and carotid arteries, during advanced atherosclerosis (4-7). It has been hypothesized that the structural defects in the IEL may play an important role during formation of atherosclerotic lesion, allowing cell migration and macromolecule transfer between the intima and the different layers of the vascular wall (4, 5). However, it is not known whether this process is also taking place in the coronary circulation at the early stage of atherosclerosis. Furthermore, prior studies have used strong digestion methods to evaluate the IEL morphology, causing digestion also of the other constituents of the vessel wall with consequent shrinkage of the IEL itself. Today, laser confocal microscopy allows in situ visualization of the IEL structure at physiologic dimension and represents an excellent method for studying specimens in whole mount preparation (8).

Since experimental hypercholesterolemia is characterized by structural and functional changes in the coronary arteries, which resemble those present in the early phase of coronary atherosclerotic development (9), we, therefore, designed this study to evaluate the ultrastructural appearance of the IEL in swine coronary arteries treated by high cholesterol diet. By the use of confocal microscopy it was possible to visualize the ultrastructure of the IEL at physiological dimension and to evaluate the pres-

ence of morphological changes both qualitatively and quantitatively using a computerized digital imaging analysis technique.

MATERIALS AND METHODS

Arterial specimens

The experiments were performed using nine female juvenile domestic crossbred pigs weighing 25-35 kg. Five pigs were placed on a normal laboratory chow diet (Group 1). Another four animals were fed with a high-cholesterol diet consisting of 2% cholesterol and 15% lard by weight (TD 93296, Harlan Tekiad) for 10 to 12 weeks (Group 2). Plasma total cholesterol and lipoproteins levels were determined by an enzymatic method previously described (10), using a commercial reagent (Roche). At the time of sacrifice, after plasma cholesterol level measurements, the animals were euthanized using an intravenous commercial euthanasia solution by the ear vein (10 mL Sleepaway, Fort Dodge Laboratories).

Tissue preparation

Immediately after removal of the heart, each heart was placed on a fixation pump and perfused with 10% formalin at 70 mmHg of pressure to maintain coronary artery morphologic integrity. Twelve coronary segments (4 left anterior descending, 4 left circumflex, and 4 right coronary arteries) from the hypercholesterolemic group and fifteen segments (5 left anterior descending, 5 left circumflex, and 5 right coronary arteries) from the control group were evaluated. After fixation, the coronary arteries were dissected from the heart, and the adventitia was removed by stripping. Then, each coronary segment, harvested from the proximal or mid-portion of the coronary artery, was cut transversely into six specimens of 2-3 mm length each. The specimen corresponding to the proximal part of the coronary segment and the specimen corresponding to the distal part of the coronary segment were excluded from the analysis to avoid artifacts due to segment manipulation. For each coronary artery, of the remaining 4 segments, one was utilized for TEM study and for histologic analysis, one for SEM study, and one for the confocal microscopy study. All coronary specimens contained no branches, which were intentionally avoided since these sites could be a source of variation in fenestrae density for the higher shear stress present at the branch points.

Transmission electron microscopy (TEM)

One specimen from each segment (hypercholesterolemic group, n=12; control group, n=15) was examined by TEM. TEM imaging was performed without the use of elastin purification treatment to measure the thickness of the IEL and to perform a morphologic examination of the intimal layer.

In brief, coronary specimens were fixed in Trump's fixative (1% glutaraldehyde and 4% formaldehyde in 0.1 M phosphate buffer, pH 7.2), and then rinsed for 30 minutes, in 3 changes of 0.1 M phosphate buffer, pH 7.2, followed by one hour postfix in phosphate-buffered 1% OsO_4. After rinsing in 3 changes of distilled water for 30 minutes the specimens were stained en bloc with 2% uranyl acetate for 30 minutes at 60℃, followed by rinsing in three changes of distilled water. The specimens were dehydrated in progressive concentrations of ethanol and 100% propylene oxide and embedded in Spurr's resin. Thin (90 nm) sections were cut on a Reichert Ultracut E ultramicrotome, placed on 200 mesh copper grids and stained with lead citrate. Semithin sections were stained with toluidine blue. Images were taken on a JEOL 1200 EXII electron microscope operating at 60 Kv. Regions of the IEL were selected and the thickness of the IEL was measured using the scale bar with a magnification of 4,000×.

Histologic examination

Toluidine blue stained cross sections were used for morphometric measurements of intimal thickness using a magnification of 4×. The thickness of the intimal layer (defined as the distance from the lumen surface of the endothelium to the inner border of the IEL) was manually traced at 8 different sites around the entire circumference of the vessel wall. A mean value was obtained for each coronary segment.

Scanning electron microscopy (SEM) and elastin purification

One specimen from each coronary segment was studied for morphological examination. Coronary specimens were immersed in 0.1 N NaOH at 70℃ for 90 minutes. This hot alkaline treatment digested and removed the smooth muscle cells, collagen fibers, fat and other connective tissue components, preserving only the fiber elastin content and allowing at the same time the fixation of the elastic fibers in their physiological shape (11). The coronary samples were removed from the hot alkaline bath and transferred into a bath containing 0.1 N NaOH at room temperature for 5 minutes, followed by rinsing in distilled water for 5 minutes, 0.1 N HCl for 2 minutes and saline solution for 5 minutes (12). The specimens were then fixed in Trump's fixative at least for one hour

and rinsed twice in 0.1 M phosphate buffer pH 7.2 (10 minutes/change), dehydrated in graded series of ethanol, and critical-point dried with liquid CO_2. Finally, the specimens were mounted with the luminal surface up and sputter coated with Au/Pd for observation under a JEOL 6400 SEM operating at 15 Kv.

Confocal microscopy

Confocal microscopy was utilized to visualize the ultrastructure of the IEL at physiological dimension on whole mounted specimens (8) and to evaluate the presence of morphological changes of IEL fenestrations. By the means of the optical sectioning abilities of the confocal microscope to obtain en face sequential images of cells at depth up to 1 mm. The coronary samples were cut longitudinally with the lumen side facing up, and placed on a glass slide with PBS solution for examination under the confocal microscope (13). Experiments were performed in duplicate and analyzed on a confocal laser scanning microscope LMS310 (Carl Zeiss Inc.) equipped with an argon/krypton laser. The IEL was visible by the means of its autofluorescence with the laser tuned to an excitation wave length of 488 nm and the emission collected through a 530/30 nm band-pass filter. A mean of four to five field images per specimen (hypercholesterolemic group, number of total fields=53; control group, n=72) were examined using a 40× neofluor lens with 1.3 n.a., digitized with a matrix of 512×512 pixels with a resolution of 0.3125 μm per pixel and a field size of 0.0256 mm^2. In each field, the entire thickness of the IEL was imaged by capturing a series of images at different optical axis of the microscope (z direction: 1 μm). A projection image of the IEL was then prepared by superimposing an average of 15 images using the LSM310 software on a IBM work station. Control experiments were performed in the same conditions. The results were analyzed independently by 2 operators who were blinded to the diet regimen with an intraobserver variability <10%.

Morphological analysis

The IEL projection images obtained by confocal microscopy were captured and digitized on a computer station (Sun Microcomputer). Quantitative morphometric measurements of the IEL were obtained using the Analyze software (Version 7.5, Biomedical Imaging Resource, Mayo Foundation). The following morphometric parameters were calculated: 1) fenestrae density in the IEL (i.e. the number of fenestrae per square millimeter of IEL surface area); 2) percentage of surface area of the IEL covered by fenestrae; 3) the minor diameter of the fenestrae. The measurements were obtained as follows. A region of interest (ROI) was manually traced to circumscribe the entire image. Then, an intensity histogram was selected, displaying the occurrence of gray levels (from black to white) within the ROI. Fenestrae areas (displayed in black) were differentiated against the white background, which represented the elastin fibers, by setting the upper and the lower threshold values for an intensity range of interest (IROI) that yielded the best identification of fenestration regions as judged by the operator. The number of pixels that composed the area surrounded by the elastic fibers (fenestration area) was then automatically counted by the computer. This value was divided by the total number of pixels within the image to obtain a percent of the surface area of the IEL covered by the fenestrations. The number of the fenestrae present within the ROI was then manually counted and divided by the total area of the ROI in order to obtain the density of the fenestrae. Finally the image was magnified on the computer screen (32×), and ten fenestrae per field were randomly selected. The number of pixels that formed the minor axis of the fenestrae was manually counted. This number was multiplied by a pixel size calibration factor (k=0.3125 μm) to obtain the minor diameter of the fenestrae. The calibration constant k was automatically calculated by the confocal microscope computer software.

Immunohistochemistry for MMP-3

Paraffin sections (5 μm) were made and transferred to glass slides. Slides were deparaffinized and rehydrated through the following solutions: xylene twice for 5 minutes, 100% ethanol twice for 10 dips and 95% ethanol twice for 10 dips. Endogenous peroxidase activity was blocked for 10 minutes at room temperature in 50% volume H_2O_2/50% volume methanol and rinsed in running tap water. Non-specific protein binding sites were blocked by applying 5% normal goat serum diluted in PBS/0.05% Tween 20 (pH=7.2-7.4) to slides for 10 minutes at room temperature. The serum was blotted off and the primary antibody (rabbit polyclonal antibodies for MMP-3, Merck Research) was diluted in 1% normal goat serum and PBS/0.05% Tween 20, applied and incubated overnight at 4℃ in a humidity chamber. On day 2, the primary antibody was rinsed off in tap water, blotted and the biotinylated secondary antisera cocktail including goat anti-mouse and goat anti-rabbit IgG diluted 1/400 was incubated on the slides for 30 minutes at room temperature. Slides were rinsed in running tap water, blotted and streptavidin-horseradish peroxidase diluted 1/500 in PBS/0.05% Tween 20 and 1% normal goat serum was applied and incubated for 30 minutes at room temperature. The slides were rinsed in tap water

and color-developed in 3-amino-9-ethylcarbazole substrate solution for 15 minutes at room temperature, then counterstained in hematoxylin for 30 seconds and covered with coverslips.

Stock solutions

Tween 20	Pierce Chemical Co
Normal Goat Serum	Dako
Biotinylated Mouse IgG	Dako
Biotinylated Rabbit IgG	Dako
Streptavidin-horseradish peroxidase	Dako
3-amino-9-ethylcarbasole	Sigma

Statistical analysis

Differences between groups in the plasma cholesterol values and in the morphometric measurements of the IEL were assessed by an one-way ANOVA test followed by Mann-Whitney U-Wilcoxon Rank Sum W test. Linear regression analysis was utilized to evaluate the relationship between intimal thickness and morphometric measurements of the IEL. A value of $p<.05$ was considered significant in all analyses. All data in the text and figures are presented as mean±SEM.

RESULTS

A significant increase in plasma cholesterol and low density lipoprotein was present in the group of animals fed with high cholesterol diet compared with the control group (Table 1).

Table 1. Lipid profile in the two experimental groups

	Control	Hypercholesterolemia
Cholesterol (mg/dL)	106±11	341±75*
Low density lipoproteins (mg/dL)	34±20	263±72*
High density lipoproteins (mg/dL)	33±2	71±6*

*$p<0.05$.

TEM analysis of the coronary arteries from control pigs demonstrated that the IEL was smooth and regular without disruption of its structure (Fig. 1A). The mean thickness of the IEL was 1.63±0.12 μm. Conversely, the IEL from hypercholesterolemic animals revealed discontinuity of the IEL (Fig. 1B), associated with a decrease in the IEL thickness when compared with the control group (0.83±0.22 μm vs. 1.63±0.12 μm, respectively; $p<0.05$). Small and fusiform gaps in the IEL of hypercholesterolemic animals, were bridged by elastin fibers. Reduplication of the IEL was observed in multiple sites. Small amount of elastin, which appeared as a thin continuous sheet, branched from the original IEL (Fig. 1B).

SEM analysis of the coronary arteries from the control group of animals revealed that the IEL was made by numerous ellipsoid fenestraes of variable size (Fig. 2A). The luminal side of the IEL always appeared smooth. On

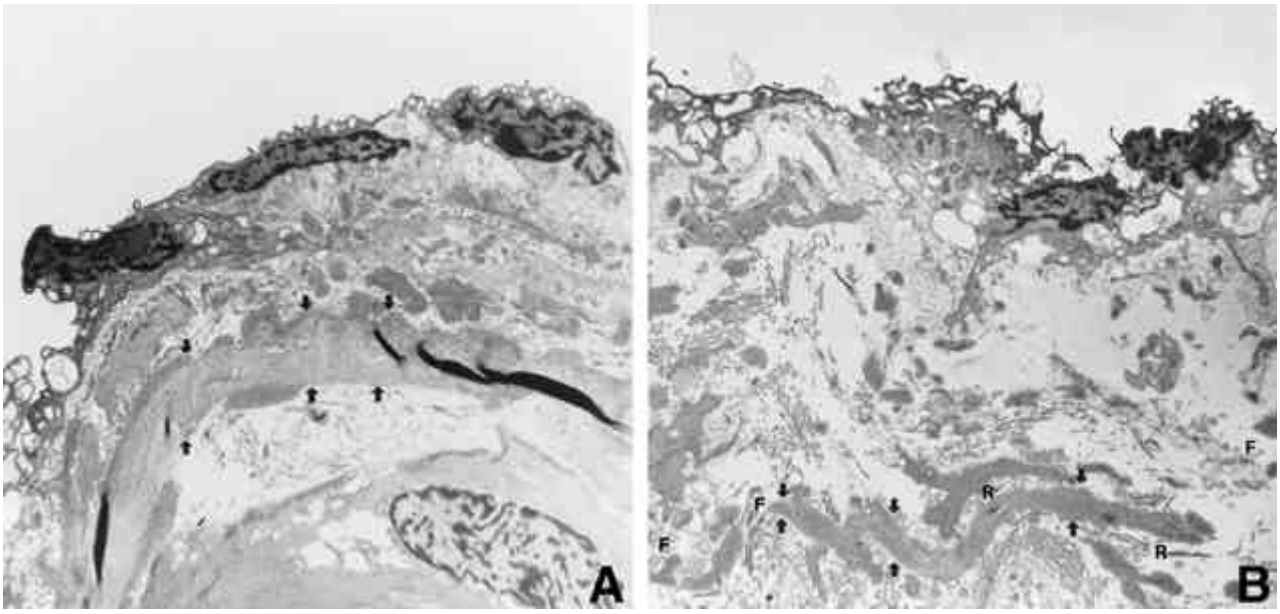

Fig. 1. Representative transmission electron photomicrographs of the IEL from a coronary artery of a control animal (Panel A) and hypercholesterolemic animal (Panel B). In control animals, the IEL (black arrow) appeared regular, smooth and without interruptions. Conversely, in hypercholesterolemic animals there was fragmentation (F) and reduplication (R) associated with thinning of the IEL (black arrow) (×4,000).

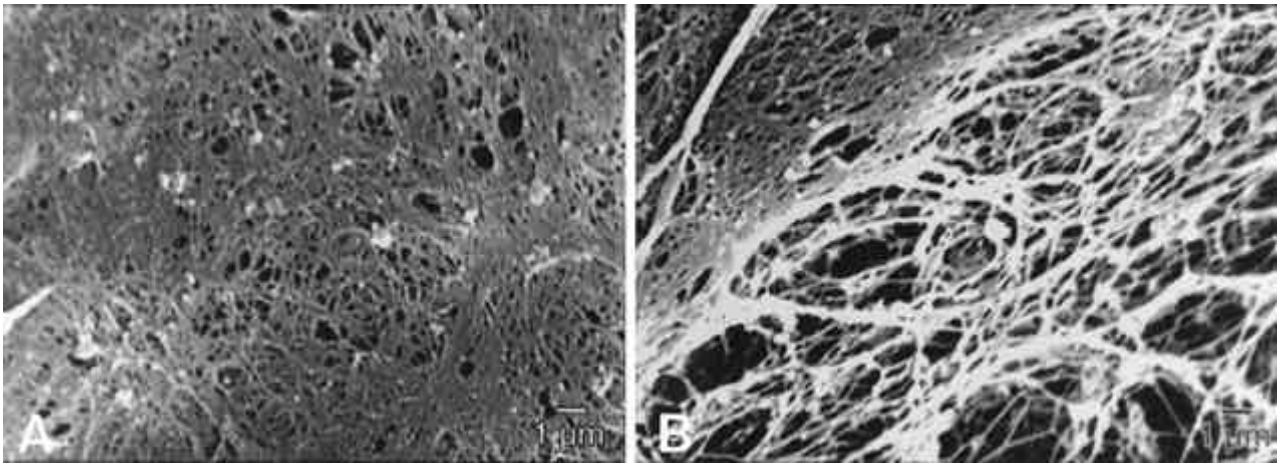

Fig. 2. Scanning electron photomicrographs of the IEL from a control (Panel A) and hypercholesterolemic animal (Panel B). Panel A shows numerous elastin fibers which run longitudinally to form small fenestrations in the IEL. In hypercholesterolemic animals, the pattern of the IEL fenestration appears altered, and larger fenestrae are observed. In the same field an area of normal IEL structure is also present (upper left corner), suggesting that the ultrastructural changes associated with hypercholesterolemia are patch distributed (×4,000).

the contrary, the luminal surface of the IEL from hypercholesterolemic pigs revealed fenestrae enlarged in size. In some hypercholesterolemic animals, fenestrae of normal size were interspersed with abnormal areas, giving the IEL a patchy appearance. An increase in the content of irregularly thickened array of elastin fibers in the intima layer was also observed (Fig. 2B).

Quantitative computerized digital analysis of the images obtained with confocal microscopy (Fig. 3), demonstrated a statistically significant increase in the minor diameters of the fenestrae in the IEL of coronary arteries obtained from hypercholesterolemic pigs compared to controls (3.32 ± 0.06 μm vs 2.16 ± 0.04 μm, respectively; $p=0.003$; Fig. 4A). This finding was also associated with a significant decrease in the density of the fenestrae in hypercholesterolemic animals ($17,552\pm931/mm^2$ vs

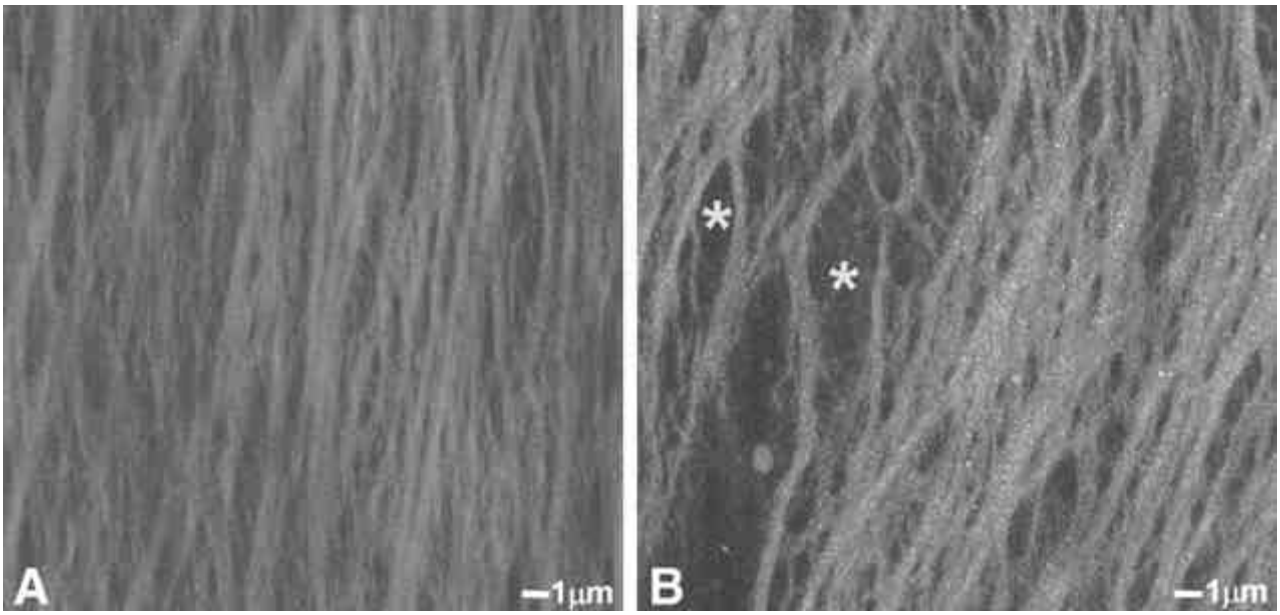

Fig. 3. Laser scanning confocal microscopic images of the IEL from a control (Panel A) and hypercholesterolemic animal (Panel B). En face images of the IEL are projections that have been created by summing serial optical sections of the same area (field size 0.0256 mm^2, ×2,560). Note the newly formed interconnections represented by transverse elastin fibers within enlarged fenestrations (*) in the hypercholesterolemic animals.

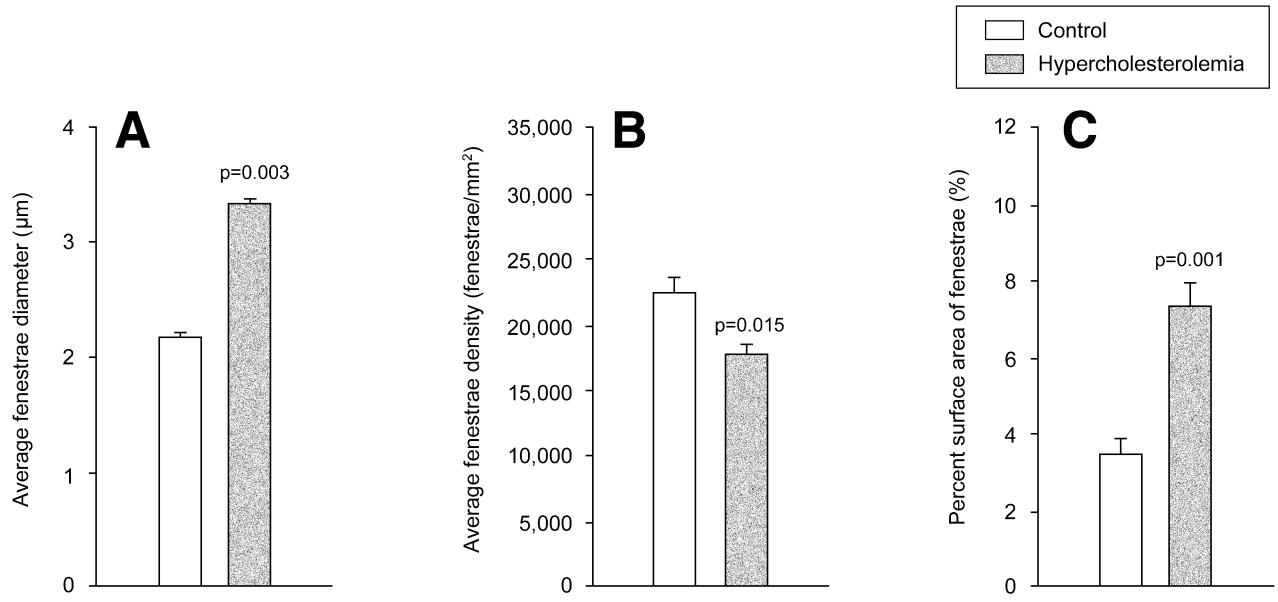

Fig. 4. Morphometric measurements obtained by quantitative computerized digital analysis of confocal microscopy images. Significant differences were observed in the diameter of the fenestrae (Panel A), fenestrae density (Panel B) and percent area of the IEL (Panel C) covered by fenestrae between hypercholsterolemic and control animals.

22,333±1,334/mm^2, respectively; p=0.015; Fig. 4B) compared with controls. Moreover, in the coronary arteries obtained from hypercholesterolemic animals, there was a significant increase in the percentage of the IEL area covered by the fenestrae compared with the control group (7.29±0.65% vs 3.49±0.37%, respectively; p=0.001; Fig. 4C).

Histomorphometric analysis demonstrated significant difference of the intimal thickness between controls and hypercholesterolemic coronary arteries (0.0271±0.0024 mm vs 0.1371±0.0130 mm, p=0.001). The percentage of the IEL area covered by the fenestrae correlated with the intimal thickness of the coronary arteries (r=0.79, p=0.004, Fig. 5).

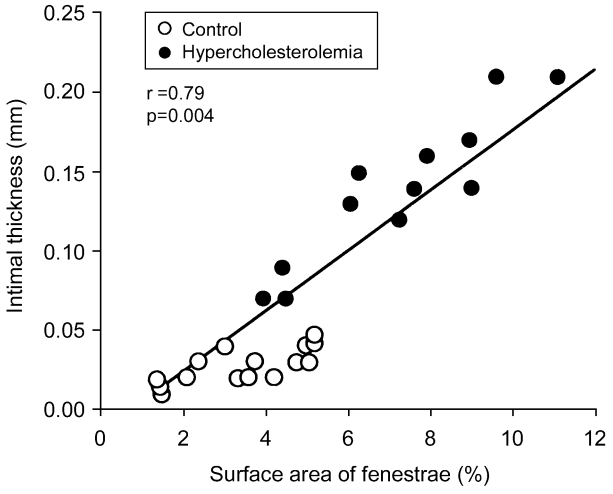

Fig. 5. Correlation between percentage of the IEL area covered by the fenestrae and the intimal thickness in the corresponding coronary segments of hypercholesterolemic (closed circle) and control (open circle) animals.

Control coronary arteries revealed little MMP-3 immunoreactivity. Within the hypercholesterolemic coronary arteries, MMP-3 immunoreactivity was evident in the neointima, media, and adventitia. Compared with control coronary arteries (Fig. 6A), hypercholesterolemic coronary arteries demonstrated marked increases in the immunoreactivity, predominantly in the neointima. MMP-3 immunoreactivity in the neointima was distributed within multi-layered elastic laminae (Fig. 6B).

DISCUSSION

This study demonstrated that in porcine coronary circulation, experimental hypercholesterolemia is associated with significant morphological and ultrastructural changes of the IEL. These changes were characterized by a decrease in the IEL thickness, an increase in the diameter and the area of the IEL fenestration. The increase in the percentage of the IEL area covered by the fenestrae was associated with a decrease in the density of the fenestrae, suggesting that fusion rather than new fenestrae formation was the major mechanism for the enlargement in the size of the IEL fenestration. The percentage of the IEL area covered by the fenestrae correlated with the

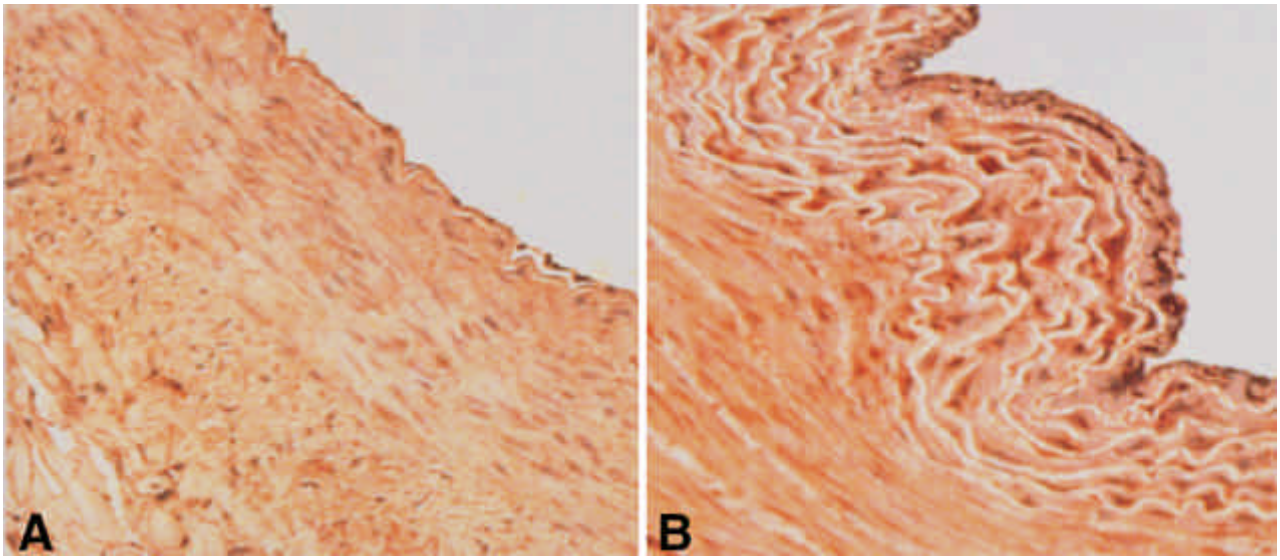

Fig. 6. Immunohistochemical demonstration of MMP-3 in control (Panel A) and hypercholesterolemic porcine coronary artery (Panel B). Compared with control coronary artery, cholesterol-fed coronary arteries demonstrated marked increases in MMP-3 immunoreactivity, predominantly in the neointima. MMP-3 immunoreactivity in the neointima were distributed within multi-layered elastic laminae, which are duplicated IEL (×20).

intimal thickness of the corresponding coronary segments. This study suggests that ultrastructural changes of the IEL induced by elastolytic activity may play an important role in the development of atherosclerotic lesion.

The arterial wall is an integrated functional component of circulatory system that is continually remodeling in response to hemodynamic conditions and disease states (8). The present study focused on the ultrastructure of IEL in the coronary arteries in the porcine model of experimental hypercholesterolemia and utilized for the first time the laser scanning confocal microscopy technique to visualize the ultrastructure of the IEL at physiological dimension on whole mounted specimens (8). Previous studies (11-12) have used strong digestion methods for elastin purification to evaluate the morphological appearance of IEL. However, with these methods, other wall constituents are also digested, therefore, causing the IEL to shrink. The present study provided in situ visualization of the IEL fixed at physiological dimensions. Such visualization was possible using laser scanning confocal microscopy, which, when operated in fluorescence mode, yielded excellent images of the IEL in whole-mount preparations (8). In addition, this method allowed us to assess the ultrastructural changes of the IEL both qualitatively and quantitatively using a computerized digital imaging analysis system.

The hypothesis that the IEL can serve as a barrier function in the vascular wall has been previously evaluated by several authors. Penn and colleagues demonstrated that the IEL was a significant barrier for penetration into the media of a macromolecule such as horseradish peroxidase (14). Those authors speculated that the role of the IEL as a barrier was greater for large macromolecule complexes, such as oxidized LDL or vector for gene transfer. Horseradish peroxidase is similar in size to some of the larger growth factors and cytokines which may cross the elastic layer of the IEL via diffusion through the fenestrae. Thus, the increase in the diameter and area of the fenestrae may contribute to the increase of the IEL permeability. It is also reasonable to hypothesize that the barrier function of the IEL may also influence paracrine communication between the endothelium and medial smooth muscle cells.

The mechanism for the ultrastructural changes in the IEL in the current study may be multifactorial. Recently, several experimental studies have shown that in response to an increased presence of mildly oxidized lipoproteins (15), which have been shown to be chemotactic for monocytes (16), an increased number of monocytes can enter the intima under hypercholesterolemic conditions (17). In addition, radiographic and electron microscopy studies have shown that macrophage foam cells are present in large numbers in the intimal layer of the vessel wall under conditions of hypercholesterolemic animals (18-20). Different studies have shown by in situ zymography and in situ hybridization that there is an expression of metalloproteinases in human atherosclerotic plaques (21-23). In particular, mRNA transcripts for MMP-3, have been localized into smooth muscle cells and macrophage foam

cells both in fibrous and lipid-rich atherosclerotic lesions (23-27). Since the lesions in experimental hypercholesterolemia resemble those present in human atherosclerosis, it may be speculated that an increased production and release of metalloproteinase from macrophage foam cells may mediate the pathologic ultrastructural changes of the IEL in this model. MMP-3, degrades proteoglycan core proteins, fibronectin, collagen, laminin, and gelatin and can activate other MMPs. MMP-3 digestion of proteoglycan core proteins can thereby enhance subsequent elastin degradation (26-29). Enhanced MMP-3 activity might contribute to the ultrastructural changes in the IEL of hypercholesterolemic coronary arteries. Such a disruption of elastin is enough to induce the migration and subendothelial proliferation of smooth muscle cells (30). Our finding is in agreement with these observations, since infiltration of macrophage foam cells in the intima was frequently found in the TEM study. In this study, the increase in the percentage of the IEL area covered by the fenestrae was associated with a decrease in the density of the fenestrae, suggesting that fusion rather than new fenestrae formation was the major mechanism for the enlargement in the size of the IEL fenestration. This hypothesis is in agreement with previous studies which have demonstrated that in elastase-treated carotid arteries, enzymatic digestion of the IEL resulted in the fusion of neighbor fenestrae (31).

Nakatake and colleagues (6, 32), and Roach and Song (33) showed that early atherosclerotic lesions of rat aorta were associated with structural changes characterized by an increase in the dome-like elastic lamina, with few fenestrae. These authors hypothesized that these changes were probably due to IEL reduplication and the increased content of elastin material in the IEL. The current study expands these previous observations principally made in elastic arteries, demonstrating that, during hypercholesterolemia, similar ultrastructural changes of the IEL also occur in muscular arteries such as the coronary arteries. Additionally, the ultrastructural defect of the IEL in the hypercholesterolemic coronary arteries correlated with the severity of intimal thickening, suggesting that these changes are strictly associated with the development of atherosclerotic lesion.

The objective of the present study was to examine the morphological ultrastructural changes in the IEL during experimental hypercholesterolemia. These changes may have an important functional significance. Fragmentation and enlarged fenestrae of the IEL may contribute to increase permeability to cells or to increase paracrine communication between the intima and medial smooth muscle cells. Further studies are needed to better understand the functional significance of the structural changes that characterize the IEL of coronary arteries in the early phase of atherosclerotic lesion formation.

REFERENCES

1. Dees MB. *On the membrane of Henles. Anat Rec 1923; 26: 161-9.*
2. Hassler O. *The windows of the internal elastic lamella of the cerebral arteries. Virchows Arch Path Anat Physiol 1962; 335: 127-32.*
3. Cook TA, Salmo NAM, Yates PO. *The elasticity of the internal lamina. J Pathol 1975; 117: 253-8.*
4. Sims FH. *Discontinuities in the internal elastic lamina: a comparision of coronary and internal mammary arteries. Artery 1985; 13: 127-43.*
5. Sims FH, Gavin JB, Vanderwee MA. *The intima of human coronary arteries. Am Heart J 1989; 118: 32-8.*
6. Nakatake J, Yamamoto T. *Three-dimensional architecture of elastic tissue in athero-arteriosclerotic lesions of the rat aorta. Atherosclerosis 1987; 64: 191-200.*
7. Rekhter MD, Andreeva ER, Mironov AA, Orekhov AN. *Three-dimensional cytoarchitecture of normal and atherosclerotic intima of human aorta. Am J Pathol 1991; 138: 569-80.*
8. Wong LCY, Langille BL. *Development remodelling of the internal elastic lamina of rabbit arteries. Circ Res 1996; 78: 799-805.*
9. Kockx MM, DeMeyer GRY, Bortier H, DeMeyer N, Muhring J, Bakker A, Jacob W, Vaeck LC, Herman A. *Luminal foam cell accumulation is associated with smooth muscle cell death in the intimal thickening of human saphenous vein grafts. Circulation 1996; 94: 1255-62.*
10. Allain CC, Poon LS, Chan CSL, Richmond W, Fu PC. *Enzymatic determination of total serum cholesterol. Clin Chem 1974; 20: 470-5.*
11. Campbell GJ, Roach MR. *Fenestrations in the internal elastic lamina at bifurcations of human cerebral arteries. Stroke 1981; 12: 489-96.*
12. Song SH, Roach MR. *Quantitative changes in the size of fenestrations of the elastic laminae of sheep thoracic aorta studies with SEM. Blood Vessels 1983; 20: 145-53.*
13. Jester JV, Andrews PM, Petroll WM, Lemp MA, Cavanagh HD. *In vivo, real-time confocal imaging. J Electron Microsc Tech 1991; 18: 50-60.*
14. Penn MS, Saidel GM, Chisolm GM. *Relative significance of endothelium and internal elastic lamina in regulating the entry of macromolecules into arteries in vivo. Cir Res 1994; 74: 74-82.*
15. Juul K, Nielsen LB, Munkholm K, Stender S, Nordestgaard BG. *Oxidation of plasma low-density lipoprotein accelerates its accumulation and degradation in the arterial wall in vivo. Circulation 1996; 94: 1698-704.*
16. Quinn MT, Parthasarathy S, Fong LG, Steinberg D. *Oxidatively modified low density lipoproteins: a potential role in recruitment and retention of monocyte/macrophages during*

atherogenesis. Proc Natl Acad Sci USA 1987; 84: 2995-8.

17. Lewis JC, Taylor RG, Jerome WG. *Foam cell characteristics in coronary arteries and aortas of white carneau pigeons with moderate hypercholesterolemia. Ann N.Y. Acad Sci 1985; 454: 91-100.*
18. Stary HC. *Proliferation of arterial cells in atherosclerosis. Adv Exp Med Biol 1974; 43: 59-81.*
19. Stary HC, Malinnow MR. *Ultrastructure of experimental coronary artery atherosclerosis in cynomolgus macaques. Atherosclerosis 1982; 43: 151-75.*
20. Stary HC, Chandler AB, Glagov S, Guyton JR, Insull W, Rosenfield ME, Shaffer SA, Schwartz CJ, Wagner WD, Wissler RW. *A definition of initial, fatty streak, and intermediate lesion of atherosclerosis. Arterioscler Thromb 1994; 14: 840-56.*
21. Henney AM, Wakeley PR, Davies MJ, Foster K, Hembry R, Murphy G, Humphries SE. *Localization of stromelysin gene expression in atherosclerotic plaques by in situ hybridization. Proc Natl Acad Sci USA 1991; 88: 8154-8.*
22. Galis ZS, Sukhova GK, Lark MV, Libby P. *Increased expression of matrix metalloproteinases and matrix degrading activity in vulnerable regions of human atherosclerotic plaques. J Clin Invest 1994; 94: 2493-503.*
23. Dollery CM, McEwan JR, Henney AM. *Matrix metalloproteinases and cardiovascular disease. Cir Res 1995; 77: 863-8.*
24. Strauss BH, Robinson R, Batchelor WB, Chisholm RJ, Ravi G, Natarajan MK, Logan RA, Mehta SR, Levy DE, Ezrin AM, Keeley FW. *In vivo collagen turnover following experimental balloon angioplasty injury and the role of matrix metalloproteinases. Cir Res 1996; 79: 541-50.*
25. Pauly RR, Passaniti A, Bilato C, Monticone R, Cheng L, Papadopoulos N, Gluzbond YA, Smith L, Weinstein C, Lakatta EG, Crow MT. *Migration of cultured vascular smooth muscle cells through a basement membrane barrier requires type 4 collagenase activity and is inhibited by cellular differentiation. Circ Res 1994; 75: 41-54.*
26. Newman KM, Ogata Y, Malon AM, Irizarry E, Gandhi RH, Nagese H, Tilson MD. *Identification of matrix metalloproteinases 3 (stromelysin-1) and 9 (gelatinase B) in abdominal aortic aneurysm. Atherosclerosis 1994; 14: 1315-20.*
27. Knox JB, Sukhova GK, Whittemore AD, Libby P. *Evidence for altered balance between matrix metalloproteinases and their inhibitors in human aortic diseases. Circulation 1997; 95: 205-12.*
28. Jones PA, Werb Z. *Degradation of connective tissue matrices by macrophages, II: influence of matrix composition on proteolysis of glycoproteins, elastin, and collagen by macrophages in culture. J Exp Med 1980; 152: 1527-33.*
29. Oho S, Rabinovitch M. *Post-cardiac transplant arteriopathy in piglets is associated with fragmentation of elastin and increased activity of a serine elastase. Am J Pathol 1994; 145: 202-10.*
30. Li DY, Brook B, Davis EC, Mecham RP, Sorensen LK, Boak BB, Eichwald E, Keating MT. *Elastin is essential determinant of arterial morphogenesis. Nature 1998; 393: 276-90.*
31. Martin BJ, Stehbens WE, Davis PF, Ryan PA. *Scanning electron microscopic study of hemodynamically induced tears in the internal elastic lamina of rabbits arteries. Pathology 1989; 21: 207-12.*
32. Nakatake J, Wasano K, Yamamoto T. *Three-dimensional architecture of elastic tissue in early arteriosclerotic lesions of rat aorta. Atherosclerosis 1985; 57: 199-208.*
33. Roach MR, Song SH. *Arterial elastin as seen with scanning electron microscopy: a review. Scanning Microsc 1988; 2: 993-1004.*